Preparation of Ordered Nano-Titania Arrays and Electrodeposition of Nano- Hydroxyapatite Crystals on Ti-6Al%-4%V Dental Implant Surfaces

Heba A. Shalaby[*1], Azza M. Hashem[2], Nadia A. Badr[2], Madiha M. Shoeib[3] and Monazzah G. Khafagy[4]

[1]Faculty of Oral and Dental Medicine, Nahda University, Bani Swif, Egupt
[2] Department of dental biomaterial, Faculty of Oral and Dental Medicine, Cairo University, Cairo, Egypt
[3]Department of Chemistry and Technology of Ceramic Materials, Head of Surface Treatment and Corrosion Control Department at Central Metallurgical Research and Development Institute, Egypt
[4]Departments of Spectroscopy, Physics Division, National Research Center, Cairo, Egypt
[*] hebashalaby_dental@yahoo.com

Abstract: Nano-titania surfaces enhance rapid biointegration at bone/ implant interfaces. In this study, nanotechnology was employed to prepare Ti-6Al-4V dental implant surface. Titanium alloy discs were anodized at room temperature and heat treated (Group1). Then, electrodeposition technique was used to coat the anodized surfaces with hydroxy-apatite (Group2) followed by alkaline hydrothermal treatment (Group3). The different surfaces were characterized by XRD, IFM, SEM and FTIR. The results showed that anodization of Ti-alloy disks led to the formation of ordered nano-tubes arrays made of titanium oxide Anatase phase which acted as a template for the precipitation of nano-hydroxy-apatite crystals. Conclusion: anodization is a simple method to prepare ordered nano-titania that promoted the electrodeposition of highly nano- crystalline bioactive HA coating.
[Heba A. Shalaby, Azza M. Hashem, Nadia A. Badr, Madiha M. Shoeib and Monazzah G. Khafagy. **Preparation of Ordered Nano-Titania Arrays and Electrodeposition of Nano- Hydroxyapatite Crystals on Ti-6Al%-4%V Dental Implant Surfaces**. Journal of American Science 2011;7(4):574-584]. (ISSN: 1545-1003). http://www.americanscience.org.

Key words: anodization, nanotitania, anatase, electrodeposition, nanohydroxyapatite.

1. Introduction:

Establishing and maintaining mature bone tissue at the bone-implant interface is crucial for osseointegration and long-term success of the implants. Many studies have focused on chemical composition and characteristics of the surface to control bone healing around dental implants. Therefore, various surface modifications have been applied to Ti-6Al-4V implants in an attempt to enhance differentiation and promote direct contact between bone and implant material. None of these modifications have established a rapidly healed and stable interface that is strong enough to support functional loading for long periods, *Brett, et al 2004*.

A thin passivation layer formed on Ti- surface is composed of smooth and dense TiO_2. Such a layer lacks desirable bioactive properties that cannot impart bone growth and strong chemical bonding. As well, there would be susceptibility for the formation of fibrous tissue that prohibits osteoblastic cells from firmly attaching onto the surface, and can cause inflammation and loosening of implant, *Salata, 2004*

Because of a nano-scaled structure of bone, it was expected that nano-structured TiO_2 would allow for an increase in bioactivity, *Alsberg et al, 2001*. Furthermore, the bioactivity and adhesion of osteoblasts on nano-grained titania and ordered nano-porous surface improved by about 20-30% compared with large-grain size ,*Garcia et al, 2002*. Recently, a novel nano-engineered surfaces were developed to provide better biological outcomes, *Brett, et al 2004*.

Titania nano-tube (TNT) arrays have attracted much attention because of their large specific surface area, favorable surface chemistry, and good biocompatibility. Among different methods used to prepare TNT such as assisted-templet method , sol-gel process and hydrothermal treatment, an electrochemical anodic oxidation was advantageous, *Ge Ruixia et al, 2008*. TiO_2 nanotubes produced by anodization are readily attached onto a titanium substrate in an ordered arrangement that is oriented and aligned perpendicular to the substrate offering much improved electron transfer, *Bayoumi et al, 2006*.

The solubility of the calcium phosphates coating into the of body fluids at the peri-implant region allow the saturation with the released ions to precipitate forming a biological apatite onto the surface of the implant, *de Groot et al, 1998 and Daculsi et al, 2003*. This layer of biological apatite contains endogenous proteins that serve as a matrix for osteogenic cell attachment and growth, *Davis et al, 2003* permitting the bone healing process around the implant and superior initial rate of osseointegration *Morris et al, 2000*. Accordingly, the biological fixation and the clinical success rate would be expected to be increased, *Geurs et al, 2002*.

Several techniques have been developed to coat metal implants surfaces with hydroxyapatite (HA); for example, plasma spraying, sputter-deposition, sol–gel coating, electrophoretic and electrochemical deposition and biomimetic precipitation. Using electrodeposition technique for Hydroxyapatite coating of Ti substrate avoid unwanted phase changes because of operating at low temperature and deposit complex architecture coating with controlled thickness. Most importantly, deposition of nano-structured HA crystals within the serrated TiO_2 nanotubes imparted higher bond strength, *Kar et al, 2006.*

Hence, this study aimed at preparing titania nano-tubes on the surface of Ti-6Al-4V alloy using anodization process prior to precipitation of HA coating via electrodeposition technique.

2. Materials and methods:

I-Preparation of the samples:

I-1-Acid etching of Ti-alloy samples:

A total number of 15 Ti-alloy disks *(Modern techniques and material engineering center-America ELI [F130-84 alloy])* representing three groups; five samples each, were utilized in this study. The disks dimensions were 6 mm in diameter and 2 mm in thickness. The disks were embedded in Epoxy resin block exposing an area of 28.3 mm^2 (πr^2). Stainless steel rod sheathed with Teflon for complete isolation when immersed in electrolyte solution was held to the block of each disk. The samples were fine polished using Emery paper starting from grit 600 to 1200 and were cleaned ultrasonically in deionized water for 5 minutes. The Ti-alloy disks were etched in mixture of 80 ml/l HNO_3, 60 ml/l HF, and 150 ml/l H_2O_2 for 5 min at room temperature. Again, the disks were ultrasonically cleaned in deionized water for 5 min and then dried by air drier.

I-2-Anodization and heat treatment of the samples:

Titania nano-tubes arrays were prepared on the disk surface by anodization. The anodization processes was carried out potentiostatically in designed electrochemical cell having two electrodes using a direct current (DC) source that was kept at constant voltage value of 20v. A platinum basket was used as cathode and Ti-alloy sample was connected as anode. The distance between cathode and anode was about 4 cm. A mixture of 1M.wt% HF and 1M H_3PO_4 aqueous solution having, pH 4.3 was used as an electrolyte, which was magnetically stirred with 120 rpm by using magnetic stirrer. The anodization process was performed for 45 min at room temperature. The samples were cleaned ultrasonically in deionized water for 5 min. Then, the samples were heat treated at 500°C for 3 hours with heating/cooling rate of 30°C/min in Muffled electric oven with automatically regulated thermocouple according to *Bayoumi et al 2005*. Five samples were kept to represent Group1 without going through the other following steps.

I-3-Electro-deposition of calcium phosphate coating:

A single component cell was used to electrochemically deposit a calcium phosphate coating. The anodized heat-treated disks of Ti-alloy were served as a cathode and platinum basket of high purity was served as anode. The used electrolyte was basically a modified simulating body fluid as referred to *Ban and Marino, 1998*. The electrolyte was prepared by dissolving 0.042 mol/l Ca $(NO_3)_2$, 0.25 mol/l $NH_4H_2PO_4$ and 1.52 gm of $MgCl.6H_2O$ in a deionized water. The pH of the electrolyte was adjusted to be 3.6-4 approximately by the addition of Tris-buffer hydroxyl aminomethan- HCL. The employed cathodic current density was 0.1mA/cm^2 supplied by DC source. The electrodeposition process was carried out for 30 min using 90 rpm magnetic stirring in accordance to *Shoeib, 2004*. Five samples subjected to this step were kept to represent Group 2.

I-4-Hydrothermal treatment:

For phase transformation of precursor of HA; Brushite, the anodized heat treated samples were subjected to hydrothermal treatment according to *Nishio et al, 2000*. The surfaces of five samples represented Group 3 were positioned above boiled 1M NaOH solution for 1hour in a properly sealed beaker to be subjected to alkaline steam.

II-Surface characterization:

Characterization of the prepared surfaces of each group was performed including identification of the composition of surface phases by X-ray diffraction (XRD) and Fourier transform infrared spectroscopic analysis (FTIR). As well, topographical study of the nanotubes surface texture with optical interference microscope (IFM) and examination of the surface morphology by scanning electron microscopy (SEM).

II-1-X- Ray Diffraction (XRD) analysis:

Thin film X-Ray diffractometer with a copper target ($Cu_{k\alpha}$ = 1.54060) and Nickel filter (PAN analytical,X'Pert Pro, Holand) was used in order to identify the constituents' phases of the disk surfaces and their average crystal size. The mathematical procedures were facilitated by computer soft ware (PSI-Plot, poly soft ware international, salt lake, UT). The data of XRD were based on Bragg's equation. The average crystal size of the constituents' phases of

the coating was calculated using Debye-Scherrer formula, *Kapczinski et al, 2003*.

II-2-Fourier Transform Infrared (FTIR) analysis:

Using (FT/6300 type A. Jasco, Japan), the infra-red spectra of the surfaces treated samples were obtained in reflection % to analyze the chemical composition.

II-3-Surface topographical study:

The length of Titania nano-tubes and their diameters were calculated by using optical interference microscope (IFM) (ZYGO Maxim-GP 200 profilometer). The evaluation of the surface roughness was carried out using surface optical profiler that traces the microstructure and topography of surfaces in three dimensions.

The selected samples were carefully ground and polished samples. Then, half of the sample surface area of the disk was isolated by a covering layer of nail polish to be electrically inconductive during the anodization according to *Vanzillotta, et al 2004*. After anodization of the exposed other half; two different regions could be clearly distinguished; an area of polished titanium-alloy surface and the other was purple in color representing anodic oxide film. Both regions were characterized by Scanning Probe Microscope (SPM) to image the topography.

II-4-Scanning Electron Microscopic (SEM) examination:

The prepared Ti-alloy disks were sputter coated with gold- palladium using Hummer 5 sputter coater. SEM was used to examine the surface morphology of selected representative samples for each group at different magnifications (JEOL JSM 5410, Japan production).

3. Results

I-Surface characterization of anodized heat treated titanium alloy (Group 1):

During the anodization process, it was observed that there was an oscillation in current density. An initial decrease in the current density occurred, and then followed by steady period and finally slight increase took place that remained constant till the end of the process. As well, there was a change in color of the sample from metallic silver to be purple. Phases were identified for anodized samples prior to and after heat treatment using (XRD). Then, surface characterization was performed using (FTIR), (IFM) and (SEM).

I-1-X-Ray diffraction (XRD) analysis:

XRD pattern of anodized Ti- alloy disks is shown in Figure (1-a). The peak values were compared with ICDD cards number 00-001-1118, 01-070-6826, and 01-071-1047 corresponding to Ti_6O, TiO_2, and Ti_2O_3 respectively. The results of anodized disks revealed that the surface was formed of these oxides. The maximum peak intensity of 100% was found at $2\theta = 40.4673^o$ and d =2.22982 for Ti_6O phase. The sharp peak of Ti_2O_3 were captured at $2\theta = 38.6050^o$, d=2.33225 and $I/I_o = 4.56\%$. Very small peak was detected for TiO_2 anatase phase at $2\theta = 47.5810^o$, d= 2.22911 with $I/I_o = 0.41\%$.

XRD of the heat treated anodized Ti- alloy disks at 500°C for 3 hours with heating / cooling rate 30°C/min is shown in Figure (1-b). ICDD 00-001-1118, 01-070-6826, 01-071-1047, and 01-072-5005 corresponding to Ti_6O, TiO_2, Ti_2O_3 and $AlTi_3$ respectively were compared with the obtained XRD patterns that revealed that the surface was formed of these oxides. The maximum peak intensity of 100% was located at $2\theta = 40.46^o$, d =2.22981 for Ti_6O phase. Sharp peaks of TiO_2 anatase were captured at $2\theta = 25.5607^o$, d=3.48503, with $I/I_o = 44.51\%$. Another two peaks were also present at $2\theta = 38.5764^o$, and d=2.3339 with $I/I_o = 37.79\%$ and $2\theta = 82.84^o$, d= 1.16531 with $I/I_o = 37.53\%$. Meanwhile only one peak for Ti_2O_3 was captured at $2\theta = 71.08^o$, d=1.32 with $I/I_o = 3.25\%$. Al Ti_3 peaks were captured at $2\theta = 63.62^o$, d=1.46403 with $I/I_o = 52.33\%$, $2\theta = 63.5921^o$, d= 1.46316 with $I/I_o = 12.21\%$ and $2\theta = 63.62^o$, d= 1.46259 with $I/I_o = 51.55\%$.

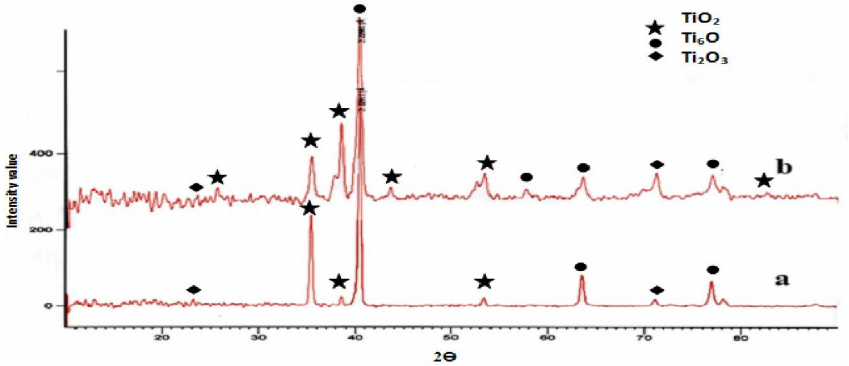

Figure1: XRD patters of anodized Ti-alloy prior heat treatment (a) and after heat treatment (b)

I-2-FTIR Spectroscopic analysis:

The analysis of FTIR spectrum of anodized Ti-alloy and heat treated disks is shown in Figure (2). The spectra revealed the presence of well defined bands of PO_4^{-3} and HPO_4^{-2} groups. The bands at 964 cm^{-1} and 1069 cm^{-1} are characteristic for symmetric vibration of PO_4^{-3} (γ_1) and asymmetric stretching vibration of PO_4^{-3}(γ_3) at 1016 cm^{-1}. A well defined band detected at 1140 cm^{-1} is characteristic for HPO_4^{-2}. The (OH^-) stretching bending vibration frequency of H_2O bands was detected at 635 cm^{-1}, 1617 cm^{-1} and 3564 cm^{-1}. The characteristic Ti-O bands were present at 663 cm^{-1}, 836 cm^{-1} and 1171 cm^{-1}.

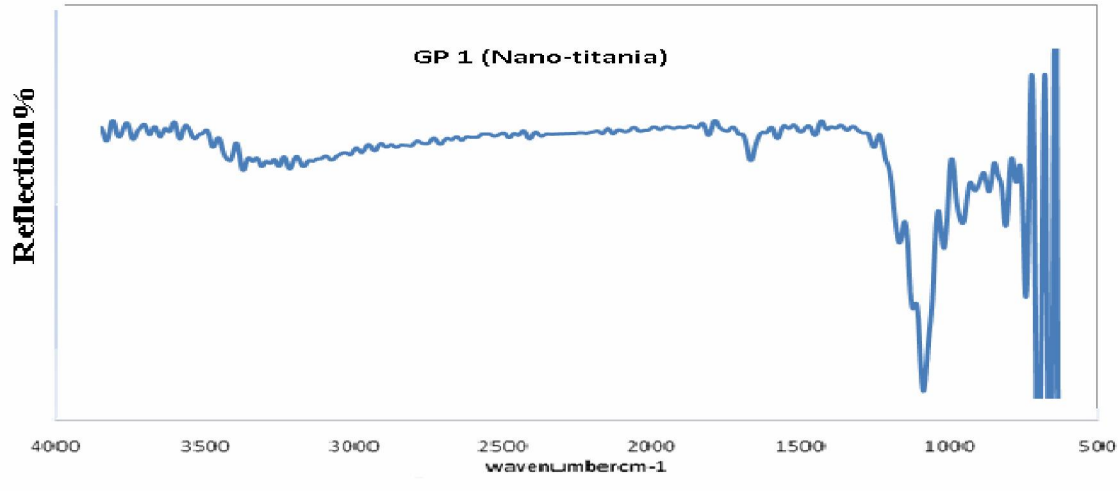

Figure 2: FTIR spectra of anodized and heat treated disks (Group 1)

I-3-Interference Microscopic examination (IFM):

Interference scanning micrograph of 2500µm^2 scanned area of heat treated anodized group is shown in Figure (3). The untreated surface; yellow and orange colored area, had Ra = 0.159 µm and Rp-v= 1.325 µm. Meanwhile the heat treated anodized surface; blue area, had 0.306 µm and 1.969 µm for the same parameters. The average nano-tubes length at that scanned area can be calculated from RP-v (anodized surface) - Rp-v (untreated surface). It was 1.969-1.325= 0.644 µm. The data analysis of surface topography of heat treated anodized group referred to untreated surface is tabulated in Table (3).

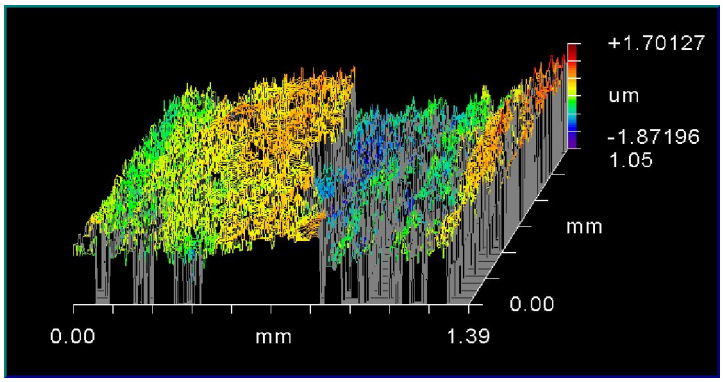

Figure -3: 3D IF micrograph of nano-titania (Group 1)

Table 3: 3D topographic parameters of 50 µm x 50 µm^2 scanning area

Scanned area	(Ra)	Rp-v
Untreated surface	158.9 nm (0.159 µm)	1.325 µm
Anodized surface	306.1 nm (0.306 µm)	1.969 µm

I-4- Scanning Electron Microscopic examination (SEM):

The surface morphology of both anodized and heat treated anodized Ti–alloy disks are shown in, Figure (4). The scanning electron micrograph of Ti –alloy disks were obtained at magnification X35000 that revealed the ultra microstructure of nano-titania oxide layer. The scanned surface is characterized by the presence of multiple, discrete well defined nano-sized pores in an ordered arrangement structure on the surface. There are pores that range from 100-150 in number spread in the scanned area; 1 μm^2, while the nano-tubes range from 45-60 nm in diameter.

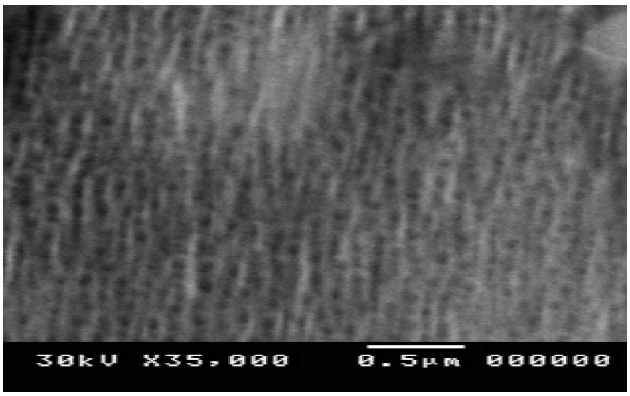

Figure-4: SE Micrographs of the prepared heat treated anodized nano-titania at magnification X35.000

II- Surface characterization of electrodeposited (Group 2) and hydrothermalalkaline treated (Group 3) HA coating:

II- 1-X-Ray diffraction (XRD) analysis:

XRD pattern obtained for electrochemical deposited layer on Ti-alloy surface (Group 2) is shown in Figure (5-a). The data was compared with ICDD card 01-080-0410 for brushite and ICDD card 01-076-0694 for hydroxyapatite. The obtained data revealed that the coating composed of different highly crystalline calcium phosphates from; mainly brushite, and hydroxyapatite. The maximum peak intensity of 100% was found at 2θ= 11.64^o and d =7.596 for brushite phase. Another sharp peaks were captured at 2 θ= 43.0872^o, d=2.099 with I/I_o= 16.77% and 2θ= 29.1092^o, d= 3.067 with I/I_o= 13.5%. The maximum peak intensity for HA was captured at 2 θ= 40.505^o, d=40.505 with I/I_o= 82.7%. Another peaks characteristics for HA were also located at 2 θ=31.9011^o, d=2.8 with I/I_o= 35.16% and 2 θ=35.39 ^{o}, d=2.536 with I/I_o= 34.04%.

XRD pattern of hydrothermally treated electrodeposited coating (Group 3) was shown in Figure (5-b). The data was compared with ICDD card 01-076-0694 for hydroxyapatite. The obtained data revealed that the coating was formed mainly from highly pure crystalline hydroxyapatite coating $Ca_5(PO_4)_3OH$, hexagonal crystal lattice. The maximum peak intensity of 100% HA was captured at 2 θ= 31.897, and d=2.8135.The other peaks were located, at 2 θ=32.632, and d=2.7668 with I/I_o= 62 %, 2 θ=35.39, and d=2.536 with I/I_o= 3.8%.

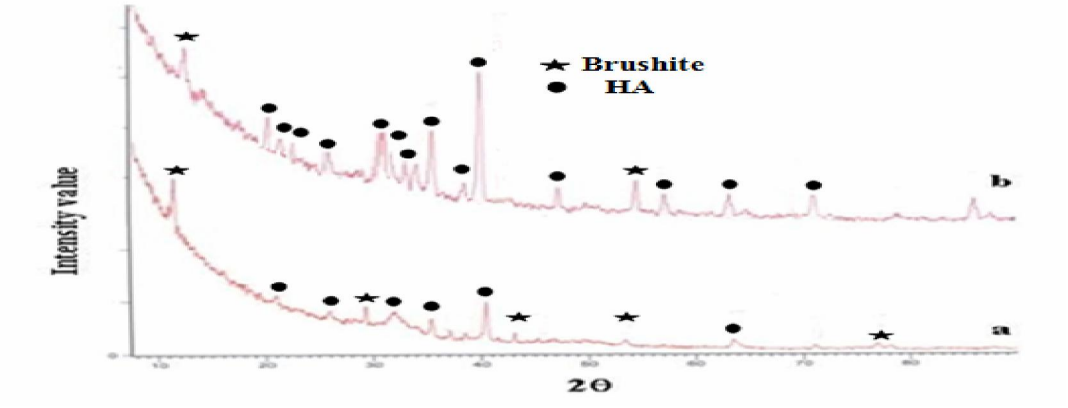

Figure 5: XRD patterns of electrodeposited calcium phosphate (a) and alkaline hydrothermally treated HA (b

II-2-FTIR spectroscopic analysis of electrochemical deposited and hydrothermally treated coating:

FTIR spectra of electrodeposited coating before and after hydrothermal treatment and their spectra analyses are shown in Figure (6).

The spectrum of Group *2* revealed the presence of well defined wide bands from 568 to 1088 cm^{-1}which are characteristic for PO_4^{-3} that occurs in stoichiometric composition of HA. Vibration band at 568 and 603 cm^{-1} are characteristics for symmetric stretching vibration of PO_4^{-3} (υ_4) while bands at 869,957 and 987 cm^{-1} are characteristic bands for symmetric stretching vibration of PO_4^{-3} (υ_1). The spectral band at 1026 cm^{-1} is characteristic for asymmetric stretching vibration of PO_4^{-3} (υ_3). The vibrational band at 1060, 1088 cm^{-1} is characteristic for symmetric stretching vibration of PO_4^{-3} (υ_3). The symmetric stretching vibrational bands of HPO_4^{-2} group are observed at 1113, 1141 and 1226 cm^{-1}. The symmetric stretching vibrational bands of CO_3^{-2} are detected at 871, 1421 and 1453 cm^{-1}. The absorbance bands characteristic for H_2O were observed at 624 and 3566 cm^{-1} which denoting OH^- group of HA.

The spectral analysis of hydrothermally alkaline treated electrodeposited coating Group 3 revealed the presence of the same well defined bands of PO_4^{-3}, HPO_4^{-2}, OH and CO_3^{-2} groups at same wave length as Group 2 but with slight shift toward the spectral inorganic region of the spectrum. The analysis of vibrational bands of CO_3^{-2} group revealed the absence of band at 1453cm^{-1}.

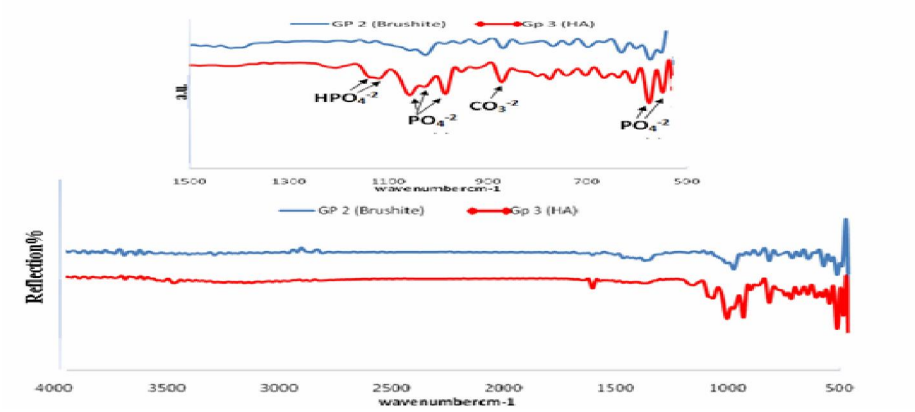

Figure (6): FTIR spectra of anodized and heat treated disks (Group 2 and 3)

II-3-SE microscopic examination:

The scanning electron micrograph of calcium phosphate electrodeposited at pH 3.6- 4 is shown in Figure (7). Thin needle like crystals arranged nearly parallel to each other forming plates having lengths ranged from 30 to 50 µm. Elongated micro-pores of 0.5-4µm size are also present between the plates.

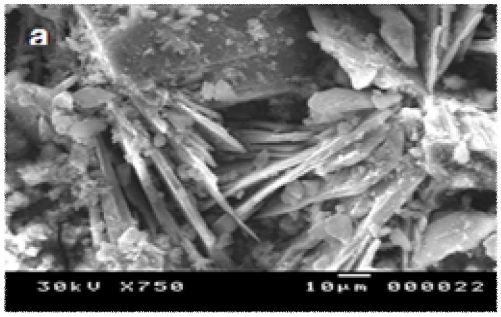

Figure (7): SE micrographs of electrodeposited calcium phosphate coating X750

The scanning electron micrograph of hydrothermally treated electrodeposited calcium phosphate coating is shown in Figure (8) that revealed densely packed needle-like crystals. The more refined structure formed of much smaller size plates indicated typical hydroxyapatite structure of nano-sized diameter. Tiny porous ultra-structure is sited as background matrix on which the crystals were precipitated.

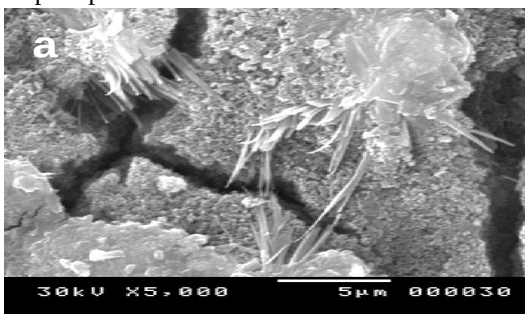

Figure (8): SE micrographs of electrodeposited calcium phosphate coating after hydrothermal treated X5000

4. Discussion:

Anodization is a controllable, reproducible and simple process to form nano-ordered tube TiO_2, *Yang et al 2004*. The fabrication of titania nano-tubes arrays via anodic oxidation of titanium in a fluoride-based solution consisted of HF and H_3PO_4 were reported by *Habazaki et al, 2007*.

1-Mechanism of nano-tubes formation:

The mechanism of nano-tubes arrays could be explained on the light of two processes: electrochemical anodization and chemical dissolution, *Xiao, et al, 2007*. During the anodization process in the current study, it was noticed that an initial current decay occurred probably due to the formation of the compact titania film followed by raising in the current due to the dissolution of that compact film. Finally, a steady state of low current was denoting due to the formation and growth of pores where the rate of the titania film formation equals the dissolution rate.

The process can be summarized as follow: (1) oxide growth at the surface of metal occurs due to interaction of the metal with O^{-2} or OH^- ions. (2) Metal ion (Ti^{+4}) migrates from the metal at the metal-oxide interface and eject under application of an electric field moving toward the oxide-electrolyte interface. (3) Chemical dissolution of the metal and oxide by the acidic electrolyte takes place during anodization. However, fluoride-containing electrolyte plays a key role in the formation of nano-tubes rather than nano-porous structure, *Tsuchiya et al, 2005*.

The instantaneous anodic current application led to the oxidation of Ti to Ti^{4+} ions according to the reaction:

$$Ti \rightarrow Ti^{4+} + 4e^- \quad (1)$$

Then, the anodic current rapidly decayed with expected formation of an oxide layer that could be related to the following hydrolysis reaction:

$$Ti^{4+} + 2H_2O \rightarrow TiO_2 + 4H^{4+} \quad (2)$$

The released H^+ ions during hydrolysis should have accumulated and F^- ions would migrate to the site of H^+ for electro-neutrality while excess F^- ions could compete for the sites of O^{2-} in the oxide. When concentrations of these ions reach a critical level at local regions, dissolution of TiO_2 would have occurred by fluorotitanic acid by the following reaction:

$$Ti^{4+} + 2H^+ + 6F^- \rightarrow H_2TiF_6\ (aq) \quad (3)$$

Dissolution of Ti cations would create negatively charged cation vacancies in the oxide and would migrate to the metal/oxide interface because of potential gradient across the oxide layer. The presence of metal cation vacancies near the oxide/electrolyte interface would facilitate the reaction (1) and Ti^{4+} could easily jump to the available vacancy sites. This event was manifested by the rise in anodic current. During this stage of anodization nano-ordered pores were nucleated on the oxide surface. A steady growth state of nano-tubular oxide layer would occur as shown in schematic illustration,

The voltage of anodization is an effective factor on the formation of the titania nano-tube arrays. Nano-tube samples prepared for 45min. at 20V anodization voltage resulted in uniform ordered nanotubes arrays grown on the top of Ti-metal substrate of 200-400 nm lengths. At low anodizing voltage, the morphology of porous film is sponge-like, with a typical pore size of 15-30nm. On contrast, an increased voltage would result in a surface of particulate nature. Further increasing of voltage would lead to the loss of that particulate appearance with discrete, hollow and cylindrical tube-like features (Ghicov et al, 2005) .

On the other hand, *Habazaki et al, 2006* specified that adding H_3PO_4 to HF electrolyte resulted in nano-granules, dot like structure. In this study, the use of 1M H_3PO_4 with 1wt% HF electrolyte formed nano-tubes. The creation of nano-tubes could be explained by delaying the accelerated dissolution effect of F^- ions by competition with PO_4^{3-} ions resulting in localized dissolution of the oxide layer (*Mor et al, 2006).*

The dissolved titanium cations can react with phosphoric acid and form phosphates as given in reactions (4) and (5). These products could precipitate and form inner wall layers in the nano-porous structure.

$$Ti^{4+} + 2H_3PO_4 \rightarrow Ti(HPO_4)_2 + 4H^+ \quad (4)$$

$$Ti^{4+} + Ti(HPO_4)_2 + H_3PO_4 \rightarrow Ti_2(PO_4)_2(HPO_4) + 4H^+ \quad (5)$$

FTIR spectral analysis of the anodized samples confirmed the presence of phosphorous species (PO_4^{3-} and HPO_4^{2-}). The presence of phosphate ions could facilitate the nucleation of calcium phosphate nano-crystals within nano-tubes. Growth of HA inside the nano-tubes would give anchoring effect to electrodeposed HA nanocrystals that would enhance the interfacial bond strength between TiO_2 and HA coating, *Kar, et al, 2006.*

The X-ray diffraction pattern of anodized Ti-alloy revealed the presence of many titanium oxides phases including Ti_6O, Ti_2O_3 and TiO_2 (anatase) with areas of amorphous titanium oxide. The distribution of the total % area of these crystalline titanium oxides was 409.58, 28.07 and 1.3 respectively. Heat treatment (500^{o}C/ 3hrs) result in alteration in the

distribution of crystals as revealed by great increase in percent of TiO_2 (anatase) to about 52 on the expense of other crystals, *Nian et al, 2006*. This can be attributed to the probable presence of high defect density (ion vacancies), which promotes metal ion dissolution, allowing thermal diffusion of ions and formation of more TiO_2 (anatase phase) and phase transformation of the amorphous into crystalline phase, *Varghese, et al, 2003*.

. XRD patterns in this study revealed crystal size of anatase phase ranged from 20-40 nm. The anatase phase is known to be much more beneficial for bone growth than the other phases as rutile phase of TiO_2 presumably because of the better lattice match with HA and smaller crystal size, *Ma et al, 2005*. Moreover, anatase phase has the highest chemisorptions capacity due to its higher surface energy, rough surface, and unsaturated oxygen bond, *Xie and Gao, 2009*.

The calculated lengths of nanotubes were about 644 nm as revealed by the IFM in agreement with *Khan , et al, 2006*. However, the SE Micrographs exhibited a wide range of the length of nanotubes that ranged from 800-1800 nm and their diameter ranged from45-60 nm.

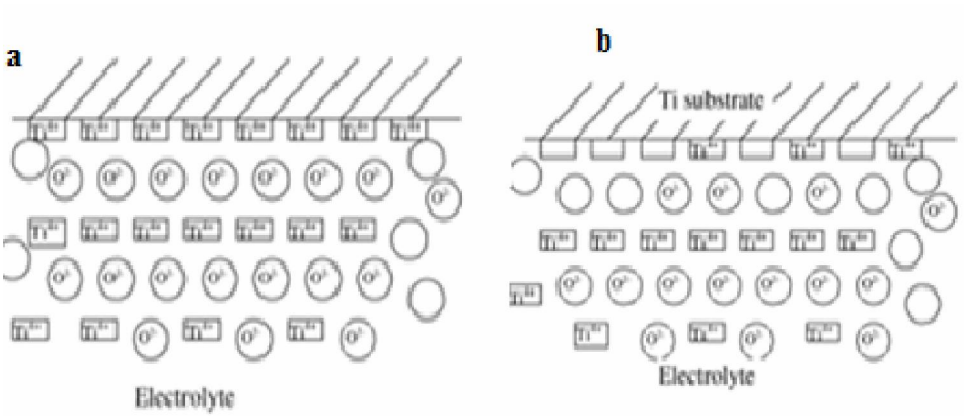

Figure (9): A schematic illustration the mechanism of nanotubes formation (a) A stable oxide indicating Ti4+ and oxygen lattice positions. Oxygen vacancies are also present; (b) Cation vacancies are transported to the metal/oxide interface

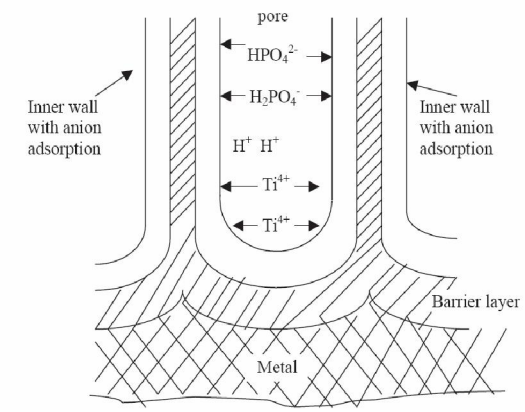

Figure (10): Cross-sectional view of the nanotubes of anodic titanium oxide layer. The outer wall of the tube (hatched portion) does not contain anions and is more of barrier-type pure oxide material. The inner wall contains adsorbed anions from the anodization solution, phosphate ions. The adsorbed phosphate ions and Ti(OH)n-xXx phase help the nucleation of calcium phosphate crystals inside the nanopores and subsequent vertical outgrowth.

2-Electrochemical deposition of nano-hydroxyapatite crystals:

When the nanotubes were cathodically polarized in a modified simulating body fluid solution containing calcium and phosphate ions, hydroxyl ions were generated on the anodized surface. *Raja et al, 2005* suggested that hydroxyl ions would be capable to transform monovalent acid phosphates into $(PO_4)^{3-}$ ions. The calcium ions would then electrostatically be attracted towards the cathodically polarized nanotubes to complete the hydroxyl apatite formation reaction. Thus, the HA crystals nucleate preferentially inside the nanotubes. The nucleation could be attributed to two reasons which are (1) the presence of phosphate ions on the inner walls of nanotubes and (2) relatively higher pH inside the nanotubes because of hydrothermal alkaline treatment of NaOH.

It was worthy to add $MgCl_2$ suggested by *Wang et al, 2003 and Yang et al, 2004* to act as nucleating agent enhancing smaller size HA crystallization on Ti-alloy surface. Moreover, modifying Ti-6Al%-4V% implant surface either by Zn, Mg or carbonated hydroxy-apatite is reported to modulate osteoblastic cell responses, *Krause et al, 2000*.

Based on theoretical chemical bases, the synthetic sequence used to produce bioceramic coatings on metallic implant surfaces is a combination of electrochemical reaction, acid-base reaction and precipitation reaction. Water is firstly reduced at the cathode surface i.e. at the surface of the implant to produce hydrogen gas and hydroxide ions, as shown in the following:

$$2H_2O + 2\bar{e} \longleftrightarrow H_2 + 2\,OH^- \text{ ---------} (1).$$

The hydroxide ions generated at the surface then may react with di-hydrogen phosphate according to equilibrium shown below:

$$OH^- + H_2PO_4^- \longleftrightarrow H_2O + H\,PO_4^{2-} \text{ ---- (2).}$$

A probable stoichiometric precipitation of mono-calcium phase ($CaHPO_4.2H_2O$); brushite, might occur:

$$Ca^{+2} + H\,PO_4^{2-} + 2H_2O \longrightarrow Ca\,(HPO_4)\,2H_2O \text{ --(3)}$$

n this study, the electric current density 0.1mA and pH 4.3 controlled the deposition rate and the morphology of synthetic intermediary brushite ($CaHPO_4.2H_2$). Then, alkaline hydrothermal treatment raised pH up to 7 that would allow transformation of brushite to highly pure HA crystals according to the following equation; *Shoeib, 2004.*

$$5CaHPO_4.2H_2O \xleftrightarrow{6Na^+} Ca_5\,(PO_4)_3OH + 10H_2O + 2Na_3PO_4 \text{ - (4).}$$

XRD pattern confirmed the chemical deposition of phosphate precursor; brushite ($CaHPO_4.2H2O$), and the presence of HA crystals. As well, the transformation of brushite to hydroxy-apatite after alkaline hydrothermal treatment with increased percentage of HA; Figure (5a and b).

FTIR analysis definited the presence of HA crystals before and after alkaline hydrothermal treatment as indicated by the presence of vibrational bands 865, 872, 960, 980,1020, 1055, 1096,1116, 1145,1225, and 1415cm^{-1}. These bands assigned for PO_4 and CO_3 groups in stoichiometric composition of mature HA Figure (6). While absence of some peaks from FTIR spectrum of prior to hydrothermal alkaline treatment proposed the nonstoichiometric composition of HA Figure (6), *Gadaleta et al, 1996.*

Thin needle like crystals arranged nearly parallel to each other forming plates having lengths ranged from and 50 to 80 nm diameter. The elongated micro-pores of size of 0.5-4 µm present between needle like plates of microscale (30-50 µm) shown in SE micrograph Figure (7) might have resulted from the generation of hydrogen bubbles produced due to cathodic reaction during electrochemical precipitation, *Nishio et al, 2000*. Meanwhile, the application of high pressure during alkaline hydrothermal treatment refined the crystals giving rise to thin needle like structure that identifying typical HA crystals in nanoscale size; Figure(8), this come in agreement with *Shoeib 2004*.

5. Conclusions:

1- A novel anodization technique was employed to create ordered nano-titania arrays on the surface of Ti-6Al%-4V% alloy.
2- Immersion in solution containing H_3PO_4 and HF during anodization produced nuclei for HA growth.
3- Heat treatment of anodized Ti-alloy surface transformed the surface oxide to the beneficial anatase phase of TiO_2.
4- Nano-titania tubes promoted the electrodeposition of highly nano- crystalline bioactive HA coating.

Corresponding author
Heba A. Shalaby
Faculty of Oral and Dental Medicine, Nahda University, Bani Swif, Egupt
hebashalaby_dental@yahoo.com

6. References:

1. Brett PM, Harle J, Salih V, Mihoc R, Olsen I, Jones FH, et al. Roughness response genes in osteoblasts. Bone ,2004;35:124–33.
2. Salata O. Applications of nanoparticles in biology and medicine. J Nanobiotech, 2004; 2:3.
3. Alsberg E,Hill E, Mooney. Craniofacial tissue engineering. Crit Rrv Oral Biol Med, 2001; 12(1): 64-75.
4. Garcia AJ, Keselowsky BG . Biomimetic surfaces for control of cell adhesion to facilitate bone formation. Crit Rev Eukaryot Gene Expr .2002: 12: 151-162.
5. Ge Ruixia, Chunjie Wang, Hongyang Zhu, Qingjiang Yu, Guangtian Zou Wuyou Fu, Haibin Yang, Yanyan Zhang, Wenyan Zhao, Zhanlian Liu.Fabrication and characterization of highly ordered titania nano-tubes via electrochemical anodization. J material letters :2008; 62:2688-2691.
6. Bayoumi Fathy, Badr G. Atya: Formation of self-organized titania nano-tubes by dealloying and anodic oxidation. J electrochemical communication. 2006; 8:3844.
7. de Groot K, Wolke JG, Jansen JA. Calcium phosphate coatings for medical implants. Proc Inst Mech Eng ,1998;212:137–47.
8. Daculsi G, Laboux O, Malard O, Weiss P. Current state of the art of biphasic calcium phosphate bioceramics. J Mater Sci Mater Med , 2003;14:195–200.
9. Davies JE. Understanding peri-implant endosseous healing. J Dent Educ, 2003;67:932–949.
10. Morris HF, Ochi S, Spray JR, Olson JW. Periodontal-type measurements associated with hydroxyapatite-coated and non-HA-coated implants: uncovering to 36 months. Ann Periodontol, 2000;5:56–67.
11. Geurs NC, Jeffcoat RL, McGlumphy EA, Reddy MS, Jeffcoat MK. Influence of implant geometry and surface characteristics on progressive osseointegration. Int J Oral Maxillofac Implants , 2002;17:811–5.
12. Filiaggi MJ, Coombs NA, Pilliar RM. Characterization of the interface in the plasma-sprayed HA coating/Ti-Al6-4V implant system. J Biomed Mater Res, 1991;25:1211–30.
13. Radin S, Ducheyne P. Plasma spraying induced changes of calcium phosphate ceramic characteristics and the effect on in vitro stability. Mater Med , 1992;3:33–42.
14. Chang YL, Lew D, Park JB, Keller JC. Biomechanical and morphometric analysis of hydroxyapatite-coated implants with varying cristallinity. J Oral Maxillofac Surg , 1999;57:1096–108.
15. Tinsley D, Watson C, Russell J. A comparison of hydroxyapatite coated implant retained fixed and removable mandibular prostheses over 4 to 6 years. Clin Oral Implant Res , 2001;12:159–66.
16. Kapczinski P.K, Gil C,Kinast E.J,Santos A.S.Surface modification of titanium by plasma nitriding.Material Research J,2003:6:265-271.
17. Kar A., K.S. Raja, M. Misra . Electrodeposition of hydroxyapatite onto nanotubular TiO2 for implant applications Surface & Coatings Technology,2006 : 201; 3723–3731.
18. Ban S, Maruno S. Deposition of calcium phosphate on titanium by electrochemical process in simulated body fluid. Jpn J Appl Phys , 1993;32:1577–80. dental materials , 2 0 0 7 ;2 3 : 844–854
19. Shoeib,M.,A.: Coating of composite materials with hydroxyapatite. Galvantechnik J. 2004; 8: 1866-1867.
20. Yang B, Uchida M, Kim HM, Zhang X, Kokubo T. Preparation of bioactive titanium metal via anodic oxidation treatment. Biomaterials , 2004;25:1003–10.
21. Mac ´ak J.M., Tsuchiya H., Schmuki P., Angew. Chem. Int. Ed , 2005: 44 ; 2100 -2102.
22. Gong D., Grimes C.A., Varghese O.K., W. Hu, R.S. Singh, Z. Chen, E.C. Dickey. J.Mater. Res, 2001:16; 3331–3334.
23. Habazaki H, Fushimi K, Shimizu K, Skeldon P, Thompson G. Fast migration of fluoride ions in growing anodic titanium oxide.Electrochemistry Communication J,2007:9:1222-1227.
24. Tsuchiya H, Macak J, Taveira L, Balaur E,Ghicov K. Self-organized TiO_2 nanotubes prepared in ammonium fluoride containing acetic acid electrolyte. Electrochem. Commun, 2005:7;576-580.
25. Xiao X, Liu R, Tian T. preparation of bioactive titania nanotube arrays in HF/Na_2HPO_4 electrolyte.J of alloys and compounds, 2007;5:1-7.
26. Ghicov A,Tsuchiya H, Macak M,Schumki P. Titanium oxide nanotubes prepared in phosphate electroloytes. Electrochemical Commun, 2005: 7:505-509.
27. Mor G,Varghese O, Paulse M, Shankar K, Grimes C. A review on highly ordered, vertically oriented TiO_2 nanotube arrays: fabrication, material properties, and solar energy applications. Sol Energy Mater. Sol. Cell J ,2006: 2011-2075.
28. Nian H,Teng H. Hydrothermal synthesis of single-crystalline anatase TiO_2 nanorods with

nanotubes as precursors. J Phys. Chem. B.110, 2006: 4193-4198.
29. Vanzillotta P.S,Soares G.A, Bastos I.N, Simao R.A,Kuromoto N.K. Potentialities of some surface characterization techniques for the development of titanium biomedical alloys.Material Research J,2004:7:437-444.
30. Varghese O.K., Gong D., Paulose M., Ong K.G, Grimes C.A, Sens. Actuators B. Vedi S, Croucher PI, Garrahan NJ, Compston JE. Effects of hormone replacement therapy on cancellous bone microstructure in postmenopausal women. Bone , 1996:19; 69-72.
31. Ma R, Fukuda K, Saaki M, Osada Y. Structure features of titaniate nanotubes/nanobelets revealed by Raman, Xray absorption fine structure and electron diffraction characterizations. J. Phys.Chem, 2005; B:109: 6210-6214.
32. Xie Xiaofeng, Gao Lian. Effect of crystal structure on adsorption behaviors of nanosized TiO_2 for heavy-metal cations.J current Applied Physics, 2009; 9:S185-S188.
33. Khan M, JungH, Yang O. Synthesis and characterization of ultra-high crystalline TiO_2 nanotubes. J Phys.Chem, 2006; B 110: 6626-6630.
34. Raja K.S., Misra T, M., Paramguru K. Deposition of calcium phosphate coating on nanotubular anodized titanium ; Materials Letters , 2005: 59 ; 2137–2141.
35. Raja K.S., Misra T, M., Paramguru K.. Formation of self-Ordered nano-tubular structures of anodic Oxide layer on titanium. Electrochemica Acta. 2005: 51:154-65.
36. Wang X, Yan W, Hayakawa S, Tsuru K, Osaka A. Apatite deposition on thermally and anodically oxidized titanium surfaces in a simulated body fluid. Biomaterials , 2003;24:4631–7.
37. Yang B, Uchida M, Kim HM, Zhang X, Kokubo T. Preparation of bioactive titanium metal via anodic oxidation treatment. Biomaterials , 2004;25:1003–10.
38. Krause A,Cowles A, Gronowicez. Integrin-mediated signaling in osteoblasts on titanium implant materials. J Biomed Mat Res , 2000;52(4):738-747.
39. Gadaleta S.j., Paschalis E.P., Betts F., Mendelsohn R., Boskey A.L. fourier transform infrared spectroscopy of solution-mediated conversion of amorphous calcium phosphate to hydroxyapatite:New correlation between X-Ray diffraction and infrared data; calcified tissue international j:1996; 58 (1) 9-16.
40. Nishio K M, Neo H, Akiyama S, Nishiguchi H,Kim M, Kokubo T, Nakamura T. The effect of alkali-and heat treatment titanium and apatite-formed titanium on osteoblastic differentiation of bone marrow cells. J Biomed Mater Res ,2000: 52(4): 652-661.

3/5/2011